Impact of Shortwave Radiative Effects of Dust Aerosols on the Summer Season Heat Low over Saudi Arabia

SAAD MOHALFI, H. S. BEDI, T. N. KRISHNAMURTI, AND STEVEN D. COCKE

Department of Meteorology, The Florida State University, Tallahassee, Florida

(Manuscript received 15 October 1997, in final form 12 February 1998)

ABSTRACT

A two-stream scattering scheme based on the delta-Eddington approximation is incorporated into the Florida State University Limited Area Model for computing the shortwave radiative fluxes due to dust aerosols over the Saudi Arabian region and to study their impact on synoptic-scale systems and the diurnal cycle over the region. The radiative properties of dust corresponding to different categories of dustiness are determined from the results of field experiments. Satellite imagery and visibility are used to determine the intensity and extent of the dust layer.

Two parallel simulations, one including the radiative effects of dust aerosols and the other without them, were made over a 6-day period starting with 1200 UTC 25 June 1979 using First GARP (Global Atmospheric Research Program) Global Experiment IIIb data analyses from ECMWF. A comparison of the two experiments shows that the dust aerosol radiative heating strengthens the heat low over Saudi Arabia. Furthermore, the radiative heating of the heavy dust concentrated at low levels during the dust outbreak episode protects the heat low from its possible destruction due to strong cold winds from the northwest.

A significant improvement in the diurnal cycle of temperature at middle levels occurs with the introduction of dust aerosols. The extension of the dust layer over the Arabian Sea also warms the middle levels in the vicinity of the dust layer and cools the layer below it, thus intensifying the inversion above the monsoon flow. The presence of dust aerosols over the Arabian Sea is also found to affect the intensity of the low-level Somali jet and the diurnal cycle of the sea breeze. These model results are found to be consistent with observations.

1. Introduction

Saudi Arabia experiences a dramatic change in weather conditions during its summer season, when the summer heat low starts to build over the region. This occurs when the large arid region extending from the northwest Indian subcontinent to the Arabian peninsula is heated at the time of onset of the Indian summer monsoon. During the First GARP (Global Atmospheric Research Program) Global Experiment (FGGE) an adequate amount of data became available on the characteristics of this heat low. One phase of the Monsoon Experiment (MONEX), a regional component of the FGGE, was the Saudi Arabian Heat Source Experiment conducted from 1 May to 15 May 1979. The goal of this phase was to investigate the heat sources at the surface and at the upper levels over Saudi Arabia and the western Arabian Sea. A high-flying National Aeronautics and Space Administration (NASA) research aircraft provided radiation measurements (upward- and downward-directed short- and longwave irradiances) and dropsonde measurements of temperature and humidity. The upper-level winds were obtained by an inertial navigation system and a number of portable automatic meteorological sensors provided surface observations over the area.

From the analysis of these data, Blake et al. (1983) noted (from observations) that the heat low over Saudi Arabia is very shallow and mostly confined to a very well-mixed layer between the surface and 800 mb. The top of the dust layer coincides roughly with the top of the well-mixed layer. An outflow layer exists near 750 mb and the air above 750 mb shows descending motions accompanied by upper-tropospheric convergence, directly above the heat low, near the 200-mb surface. The maintenance of this thermal stratification appears to be aided by the dry convection and radiation in the mixed layer and by the subsidence in the upper region. The heat budget over the region suggested the need for continual energy import over the upper troposphere via teleconnection with neighboring rain areas, especially the monsoon. Such coupling results from east–west divergent overturning with rising motion over the convective regions of the monsoon and descending motion over the deserts of Saudi Arabia.

A study by Ackerman and Cox (1982) showed that dust aerosols are a significant factor for radiative warming below 500 mb due to shortwave absorption but they

Corresponding author address: Dr. T. N. Krishnamurti, Dept. of Meteorology, The Florida State University, Tallahassee, FL 32306-4520.
E-mail: tnk@io.met.fsu.edu

have less effect on longwave radiation. They also noticed that dust approximately doubles the shortwave radiation absorption under clear-sky conditions. A similar dust aerosol warming was noticed by Smith (1986), who found it to be an important factor in balancing the radiative sink over the region. In a recent study on the radiative effect of dust aerosols, Tegen et al. (1996) have shown that dust from the disturbed soils causes a net cooling at the surface accompanied by an increase in atmospheric heating. Such radiative effects are found to be most pronounced over the Arabian region.

The above and some other studies provide understanding of the characteristics of the summer heat low, dust layer, and the radiative heat balance over the region. But they do not provide sufficient understanding of the impact of dust aerosols on the atmospheric circulation of the region. There are very few studies that have examined the effect of dust aerosols on the synoptic-scale system of this region. Among those, Karyampudi and Carlson (1988) studied the effect of Saharan air layer on easterly wave disturbances. The purpose of the present study is to examine the effect of dust aerosols on the synoptic-scale systems over the Saudi Arabian region. This is achieved using the Florida State University (FSU) Limited Area Model. This model contains parameterizations of various components of physics and has been used for many limited-area studies (Krishnamurti et al. 1990). However, the radiative parameterization scheme does not address the effect of dust aerosol, although it includes the effect of water vapor, ozone, carbon dioxide, and clouds. For the purpose of this study the radiation package was modified to include radiative effects of dust aerosol based on the two-stream Delta-Eddington approximation of the radiative transfer equation. The data collected during the MONEX field phase and satellite imagery are used to determine the extent of the dust layer. Two sets of model experiments, one including the dust aerosol radiative effects and the other without, are made to investigate the effect of dust aerosols on synoptic-scale systems.

2. Radiative transfer considerations

Under the plane-parallel assumption, the radiative transfer equation for the diffuse intensity may be written as

$$\mu \frac{dI(\tau, \mu, \theta)}{d\tau} = -I(\tau, \mu, \theta) + J(\tau, \mu, \theta). \quad (1)$$

Here, $I(\tau, \mu, \theta)$ is the intensity of a pencil of diffuse radiation in the direction (ϕ, θ) at optical depth τ. Here ϕ and θ are the zenith and azimuthal angles and $\mu = \cos\phi$. Consistent with Eq. (1), μ is regarded as positive for a radiation beam passing (across a horizontal plane) from above and negative for one coming from below. The optical depth is given by

$$\tau = \int_z^\infty k_d \, dz', \quad (2)$$

where k_d is the volume extinction coefficient. Here $J(\tau, \mu, \theta)$ is the source function due to the multiple scattering of diffuse intensity, scattering of direct solar radiation, and emission by the atmosphere. As compared to the direct solar and scattered intensity, the radiance emitted by the atmosphere can be neglected. With this the source function may be written as

$$J(\tau, \mu, \theta) = \frac{\tilde{\omega}}{4\pi} \int_0^{2\pi} \int_{-1}^{1} I(\tau, \mu', \theta') P(\mu, \theta; \mu', \theta') \, d\mu' \, d\theta' + \left(\frac{\tilde{\omega}}{4\pi} S_0 e^{-\tau/\mu_0} \right) P(\mu, \theta, \mu_0, \theta_0). \quad (3)$$

The first term on the right-hand side of Eq. (3) is the contribution of multiple scattering of diffuse radiation; the second term is due to single scattering of direct solar radiation. Here $P(\mu, \theta; \mu', \theta')$ is the phase function describing the angular distribution of scattered radiation as a function of scattering angle—for example, the proportion of radiation coming from direction (μ', θ') scattered to direction (μ, θ). Here $\tilde{\omega}$ is the single-scattering albedo defined as the ratio of the scattered radiation to the total (scattered plus absorbed) radiation.

If we assume the diffused intensity and the phase function to be independent of the azimuthal angle, then using (3) the radiative transfer equation (1) takes the form:

$$\mu \frac{dI(\tau, \mu)}{d\tau} = -I(\tau, \mu) + \frac{\tilde{\omega}}{2} \int_{-1}^{1} I(\tau, \mu') P(\mu, \mu') \, d\mu' + \frac{\tilde{\omega}}{4\pi} S_0 P(\mu, \mu_0) e^{-\tau/\mu_0}. \quad (4)$$

The heating rates due to dust aerosols are obtained by solving Eq. (4) numerically using the two-stream Delta-Eddington approximation (Joseph et al. 1976; Coakley and Chylek 1975; Meador and Weaver 1980) and dividing the atmosphere into a number of layers as defined by the vertical structure of the FSU Limited Area Model. Under the two-stream approximation, the radiative intensity and phase function are considered to be composed of a sum of symmetric and asymmetric components. The symmetric component is independent of zenith angle and the asymmetric component is proportional to the cosine of the zenith angle. The appendix provides a detailed description of the two-stream Delta-Eddington approximation and numerical solution of the radiative transfer equation (4).

3. Dust-layer characteristics and radiative heating

To calculate the radiative heating due to dust aerosols, it is required that aerosol properties such as optical depth

TABLE 1. Dust aerosol characteristics.

Dust category	Spectral interval (μm)	Extinction coefficient km^{-1}	Absorption coefficient km^{-1}	Single-scattering albedo	Asymmetry factor
Light dust	0.40	0.224	0.056	0.751	0.791
	0.55	0.229	0.048	0.791	0.773
	0.70	0.230	0.040	0.825	0.757
Moderate dust	0.40	0.945	0.277	0.706	0.841
	0.55	0.949	0.236	0.750	0.838
	0.70	0.956	0.269	0.718	0.845
Heavy dust	0.40	2.182	0.573	0.737	0.793
	0.55	2.232	0.496	0.777	0.778
	0.70	2.255	0.424	0.817	0.763

(τ), single-scattering albedo ($\tilde{\omega}$), asymmetry factor (g) and surface albedo, as well as their space and time variations, are known. These parameters depend upon the dust aerosol characteristics such as density and size distribution and refractive index, which can be determined from field experiments. In recent years, many experimental studies have been conducted to assess such properties of dust aerosols. These include the Barbados Oceanographic and Meteorological Experiment over the Atlantic Ocean during 1969, the USSR-USA dust aerosol experiment over central Asia in Tadzhikistan during 1987, and the aircraft measurements of dust aerosols over Saudi Arabia and adjacent regions during the summer MONEX of 1979 (hereafter, MONEX-79). Studies based on the Mei scattering theory utilizing data obtained from these experiments have provided knowledge about optical properties of dust aerosols like single-scattering albedo, asymmetry factor, and extinction coefficient (Carlson and Benjamin 1980; d'Almeida 1987; Ackerman and Chung 1992).

Following d'Almeida (1987), the atmospheric dustiness was classified into three categories based on horizontal visibility range as follows:

1) Light dust—visibility range greater than 7 km,
2) Moderate dust—visibility range between 2 km and 7 km, and
3) Dust storm—visibility range less than 2 km.

The optical properties for these three categories of dust aerosol given by d'Almeida (1987) and used in this study, are summarized in Table 1 for the spectral bands 0.40, 0.55, and 0.70. As supported by observations, the dust layer was assumed to be well mixed with a constant aerosol mixing ratio from the surface to the top of the dust layer. The calculations by Ackerman and Chung (1992), based on measurements over Saudi Arabia during the summer portion of MONEX, show that the single-scattering albedo and asymmetry factor are constant with height within the measurement errors. So in our study we have taken them to be a constant value over the whole depth for a given dust category.

The dust aerosol parameters given in Table 1 corresponding to the spectral wavelength 0.55 μ were used for this study. Dust aerosol heating effects by Carlson and Benjamin (1980) and Sokolik and Golitsyn (1993) were calculated with reference to similar wavelengths. The optical depth was calculated based on the extinction coefficient in Table 1. Depending on the dustiness category and thickness of the dust layer the optical depth ranged from 0.5 to 3.0. This is in agreement with d'Almeida (1987), who observed τ to be 12.8–3.4 during a dust storm, 1.0–2.5 in moderate dust conditions, and 0.4–0.5 in light dust conditions.

The present study concerns dust (*Shamal*) episodes that occurred during late June 1979. A severe dust storm affected the region for about 7 days from 22 June to 28 June 1979, followed by a 3-day break from 29 June to 1 July 1979 before another dust outbreak began. The start of the dust outbreak was associated with the intensification of a heat-low over Saudi Arabia with a trough extending northwestward toward Iraq, Syria, and Turkey. Concurrently, a Mediterranean ridge extended to the south of Jordan, northwest of Saudi Arabia, and north of the Red Sea. This caused a tight pressure gradient and strong northwesterly winds, which resulted in the onset of this dust episode. Figure 1 shows the mean sea level pressure and 850-mb winds associated with the start of this dust episode. The vertical and horizontal extents of the dust layer during the period were assessed from the vertical distribution of potential temperature provided by research aircraft and dropsonde observations, the horizontal visibility observations, and satellite imagery. In the absence of quantitative data on the intensity and extent of the dust layer, this was possibly the best way to estimate the extent of the dust layers. The advection of dust aerosol from Saudi Arabia to the adjoining sea area was also measured by research aircraft. Figure 2 shows the vertical distribution of potential temperature at 1200 UTC from 26 June to 1 July 1979 over points located over the northern, central, and southern Saudi Arabian peninsula and northeast Arabian Sea. Over the Saudi peninsula the dust layer is found to be well mixed with the top extending to 700–650 mb over the northern parts and to about 600 mb over its central and southern parts. A low-level inversion at about 900 mb, which coincides with the base of the dust layer, is observed during the first 3 days, which weakens and disappears as the layer becomes well mixed during

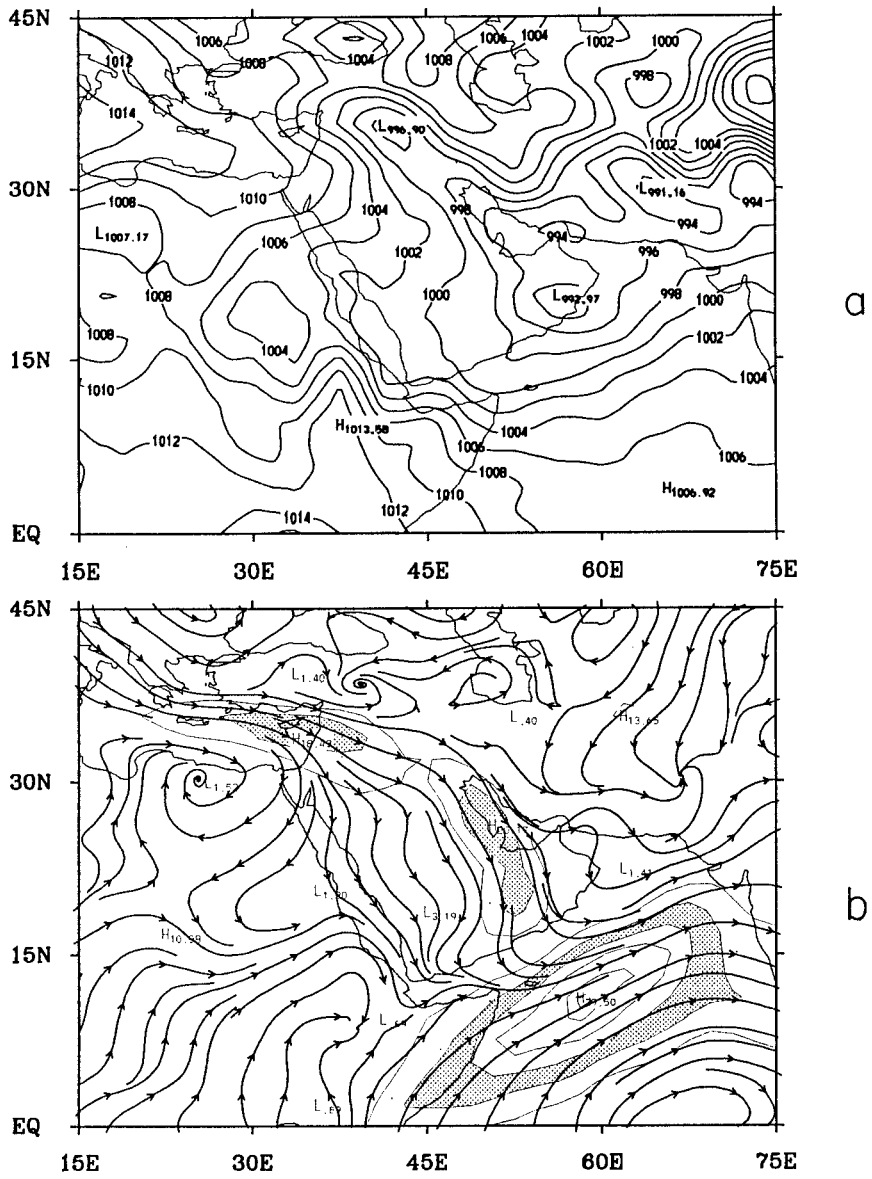

FIG. 1. (a) Mean sea level pressure (mb) and (b) 850-mb wind field at 1200 UTC on 22 June 1979, at the start of dust episode.

the next 3 days. Over the Arabian Sea the dust layer is relatively less mixed with the base at 900 mb and the top at 700 mb during the first 3 days and appears to have weakened toward the end of the period.

Figure 3 shows the horizontal extent of the base and the top dust layer as well as its thickness at 1200 UTC on 26 June and 1 July 1979, the beginning and end of the dust episode. In the beginning the dust layer is confined mainly to the Saudi Arabian Peninsula with the lowest base at 950 mb over the central parts and its highest top at 600 mb over the southern parts of the peninsula. The dust layer is spread northwestward and southeastward by the prevailing low-level winds from Syria and northern Iraq in the northwest to the western parts of India in the southeast. The thickness of the core of the dust layer also increases from 300 mb to 350 mb during this period. The vertical and horizontal extension of the dust layer mainly occurred during the last 3 days of the dust period.

The above characteristics of the dust layer provided the necessary data on the basis of which the single-scattering albedo ($\tilde{\omega}$), the asymmetry parameter (g), and the optical thickness (τ) were incorporated into the dust aerosol radiation packages of the FSU Limited Area Model. Following Joseph et al. (1976) and Carlson and Benjamin (1980), these parameters were modified before their use in the Delta-Eddington radiative transfer calculations as follows:

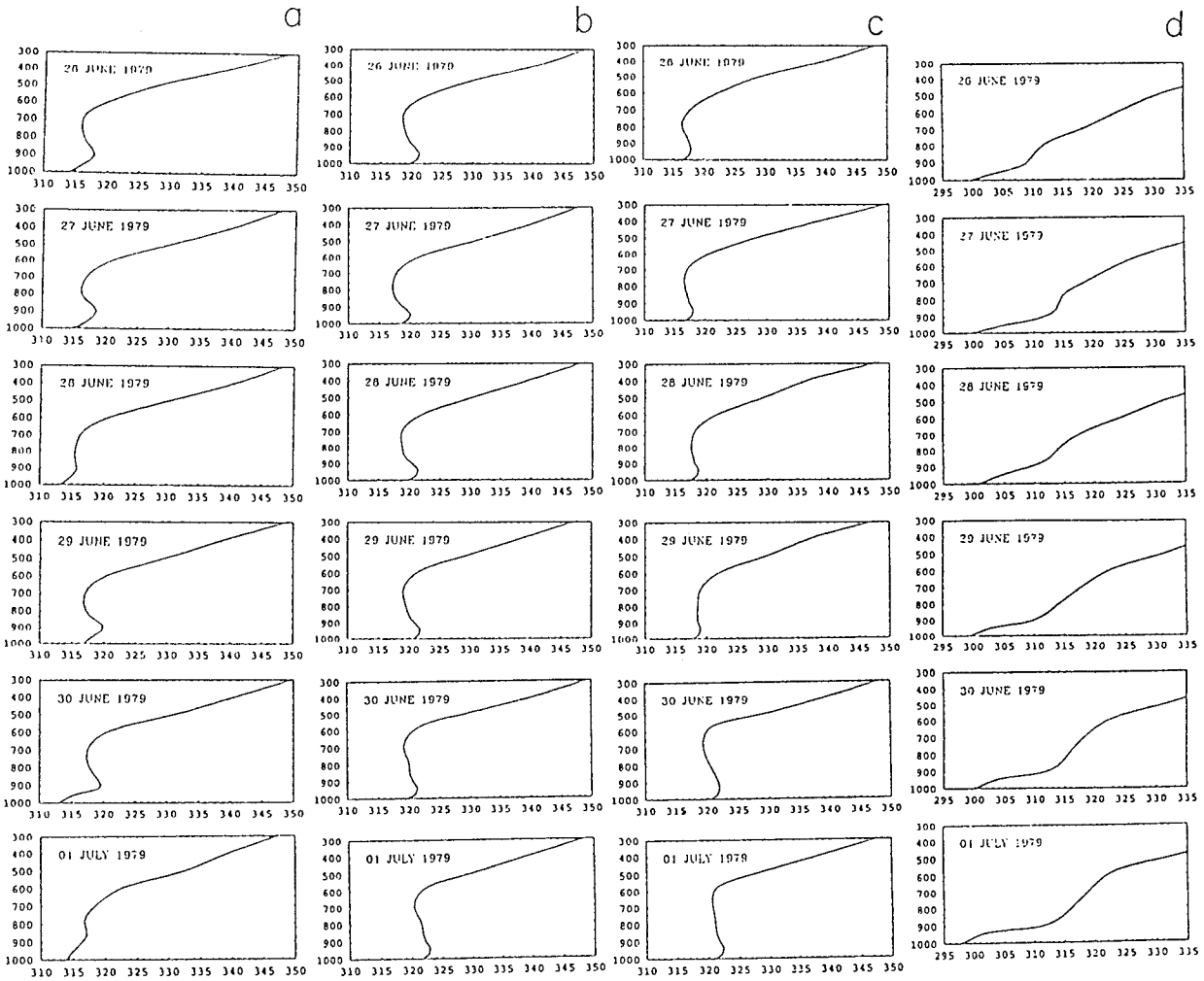

FIG. 2. Vertical distribution of potential temperature at 1200 UTC from 26 June to 1 July 1979 over points located at: (a) northern Saudi Arabia (30°N, 43°E) (b) central Saudi Arabia (24°N, 48°E) (c) southern Saudi Arabia (19°N, 52°E), and (d) the northeast Arabian Sea (19°N, 60°E)

$$\tau = (1 - \overline{\omega}^* g^{*2})\tau^*, \tag{5a}$$

$$\overline{\omega} = \frac{(1 - g^{*2})\overline{\omega}^*}{(1 - \overline{\omega}^* g^{*2})}, \tag{5b}$$

$$g = \frac{g^*}{1 + g^*}, \tag{5c}$$

where τ^*, $\overline{\omega}^*$, and g^* are the actual values and τ, $\overline{\omega}$, and g are the scaled values of optical thickness, single-scattering albedo, and asymmetry parameter, respectively.

The FSU Limited Area Model used in this study has been used previously for many limited-area studies and is described in detail in Krishnamurti et al. (1990). It has a comprehensive parameterization of physical processes, such as deep convection based on a modified Kuo scheme (Krishnamurti et al. 1983), boundary layer fluxes of moisture and momentum based on similarity theory (Businger et al. 1971), and short- and longwave radiation (Harshvardhan and Corsetti 1984; Lacis and Hansen 1974). The parameterization of short- and longwave radiation includes the radiative effects of water vapor, carbon dioxide, ozone, and clouds. The low, medium, and high clouds for cloud–radiation interactions were specified from the threshold values of predicted relative humidity. The surface albedo over Saudi Arabia was based on field observations during MONEX-79. Similar to Ackerman and Cox (1982), a value of 0.4 was used for the Saudi Arabian desert region. Over the neighboring land and ocean areas, surface albedo climatology for the summer season was used. The surface temperatures over land are determined through the radiative heat balance over land surfaces, whereas over the ocean areas the sea surface temperatures are prescribed. The model, however, does not include the calculation of radiative effects of aerosols on a routine basis, which is the subject of this study.

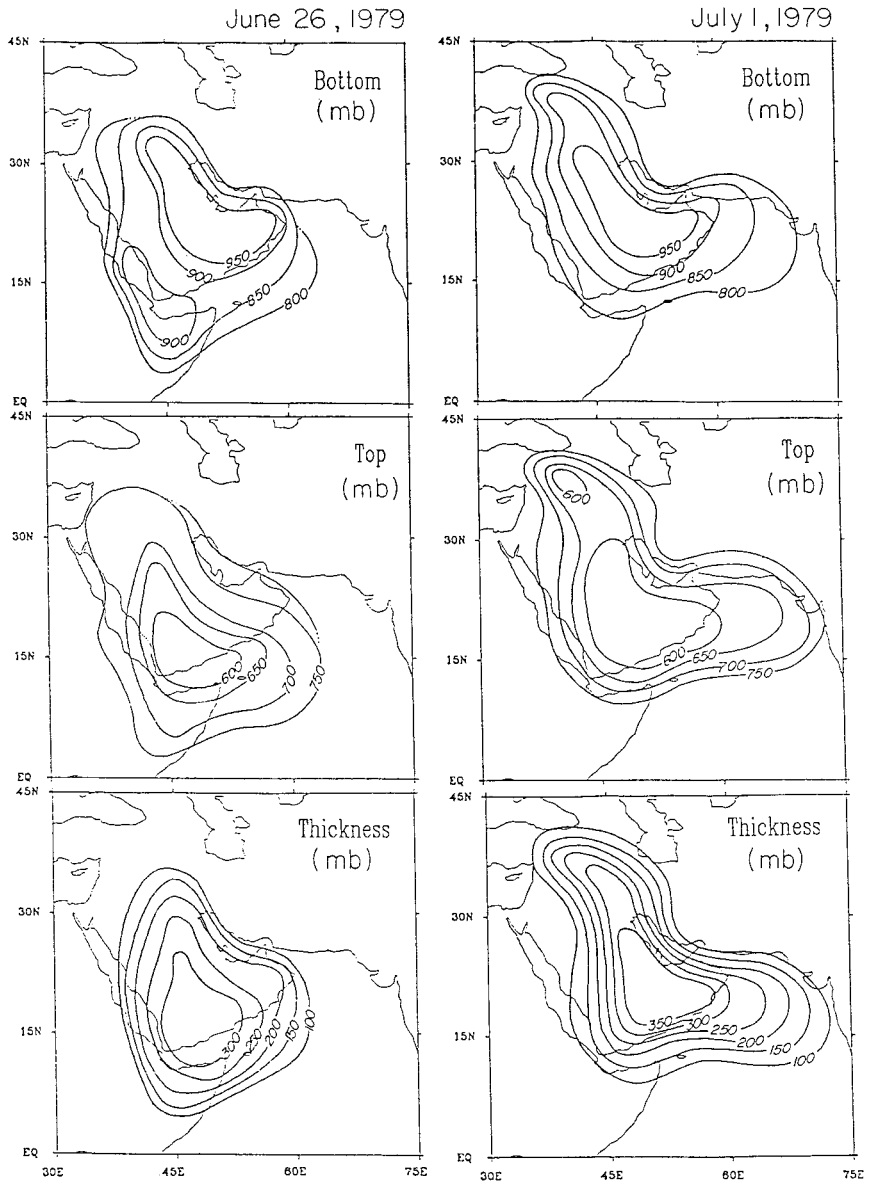

FIG. 3. Horizontal extent of the top, base, and thickness (in mb) of dust layer at 1200 UTC on 26 June and 1 July 1979

The model has a horizontal resolution of 0.5° lat × 0.5° long with 15 layers in the vertical as shown in Fig. 4. This resolution is adequate to capture regional synoptic-scale features. Starting from 1200 UTC on 25 June 1979, the model was integrated for 6 days using the FGGE IIIb analysis from the European Centre for Medium-Range Weather Forecasts. Two parallel runs were made starting with the same initial input data. The control experiment used the normal physics parameterization package without dust aerosol radiative effects. The parameterization of physical processes in the aerosol experiment was similar to that in the control experiment, except that in addition it included the shortwave radiative effects of aerosol.

It was necessary to verify model-produced dust aerosol heating against observation before investigating its impact on regional synoptic-scale systems. The observed fluxes obtained (by the NASA *CV900* aircraft) over the Saudi Arabian deserts during a daytime flight mission on 10 May 1979 (Smith et al. 1980; Ackerman and Cox 1982) were used to calculate observed heating rates of the dust-laden atmosphere. The heating rates without dust aerosol effects (but all other effects included) were calculated from the radiation package of

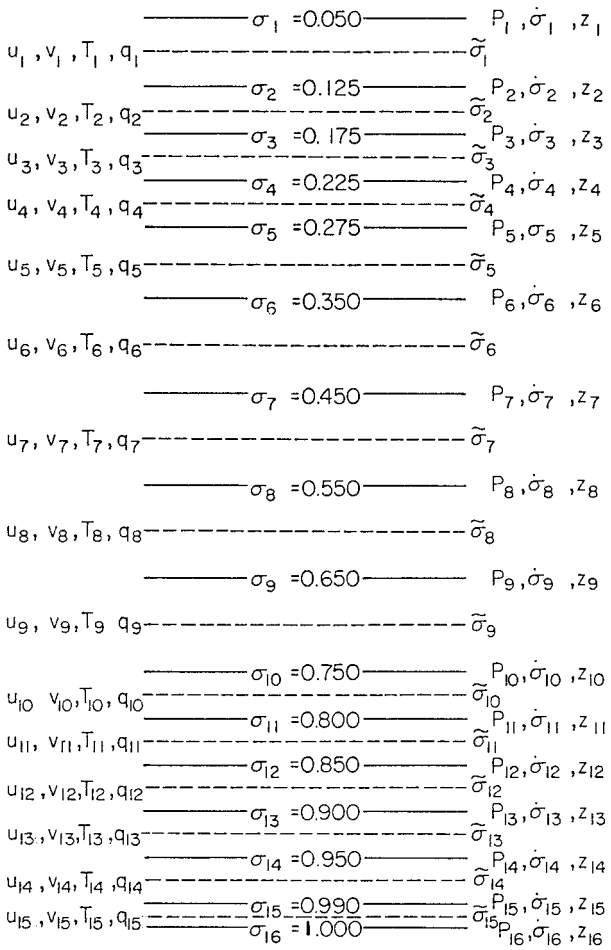

FIG. 4. Vertical resolution of the FSU Limited Area Model.

the FSU model before incorporating dust aerosol effects. The temperature, relative humidity, and surface albedo used in these calculations were obtained from the dropsonde and onboard measurements from the same flight mission. The difference between observed and model heating rates provides an estimate of dust aerosol radiative effects.

Figure 5 shows thus obtained estimates of shortwave and longwave heating rates due to dust aerosols. These are obtained as the difference between shortwave and longwave heating rates observed during MONEX (which included the effect of dust aerosols) and corresponding heating rates obtained from FSU radiation code without including radiative effects of dust aerosols. Although dust aerosols appear to have a minor effect on longwave radiation, they have a significant effect on the shortwave radiation by heating the atmosphere up to 3°C day^{-1}. The vertical distribution of heating rates shows that the shortwave heating rates are nearly uniformly distributed over the depth of the dust layer between 900 mb and 600 mb. The decrease of shortwave warming below 900 mb reflects the effect of the dust

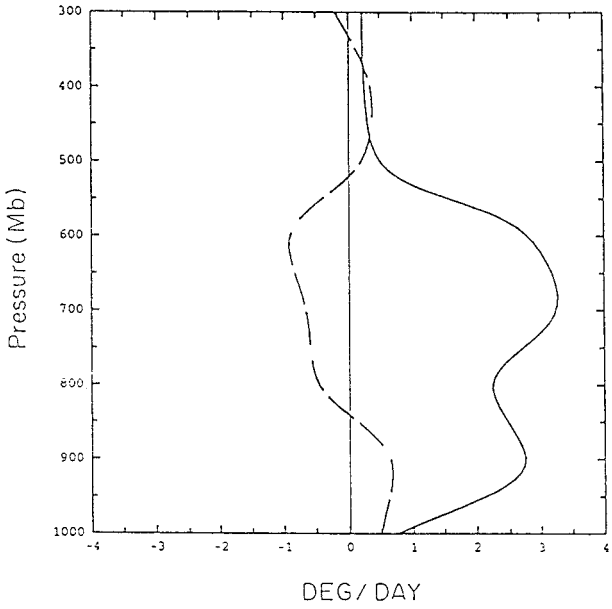

FIG. 5. Difference between the shortwave and longwave heating rates of the dust laden atmosphere from MONEX 1979 data, and those for the dust-free atmosphere calculated from the FSU model. These provide estimates of shortwave (solid line) and longwave (dashed line) heating rates due to dust aerosols. Units: degrees day^{-1}.

in reducing the incoming solar radiation at the surface. Similar results for the solar spectrum radiative heating over the desert of Saudi Arabia were obtained by Ackerman and Cox (1982) and Ackerman and Chung (1992), and over the Saharan desert by Carlson and Benjamin (1980).

Figure 6 shows the aerosol radiative heating rates calculated as a function of total dust optical depth (τ_d) based on the Delta-Eddington approximation. The figure shows that with an increase of the dust optical depth, the radiative heating also increases throughout the dust layer. The maximum heating of 3.0°, 4.5°, and 6.5° C, corresponding to τ_d of 0.5, 1.5, and 3.0, respectively, occurred at 600 mb, near the top of the dust layer. The heating rate was nearly uniform with height for the lower optical depth, $\tau_d = 0.5$, whereas it increased with altitude as the optical depth increased to a value of $\tau_d = 3$. This is consistent with the findings of Carlson and Benjamin (1980) and Sokolik and Golitsyn (1993).

The present study concerns only the shortwave radiative effects of dust aerosols, which are much stronger than their longwave radiative effects, though some studies show that longwave effects may also contribute to some significant extent (Tegen et al. 1996).

4. Impact of dust aerosols on regional synoptic systems

The impact of dust aerosol radiative effects on synoptic-scale systems is studied by examining the differences between the forecasts based on

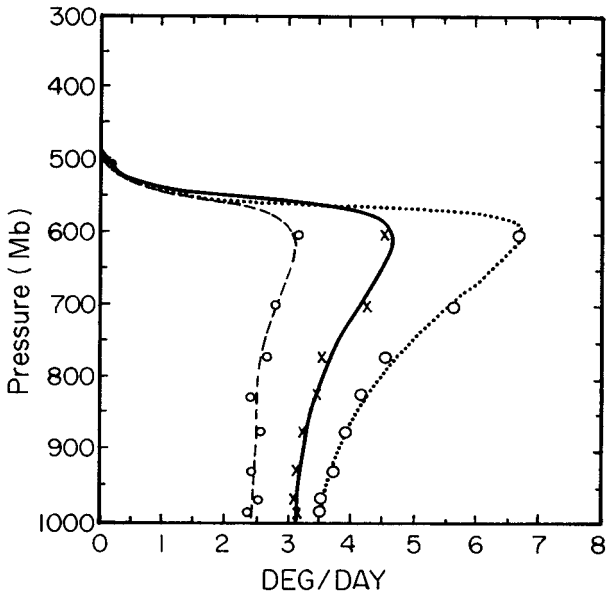

FIG. 6. Vertical distribution of shortwave heating rates due to dust aerosols at noon over the Saudi desert as function of the aerosol optical depth (τ_d) for $\tau_d = 3$ (dotted line), $\tau_d = 1.5$ (solid line), and $\tau_d = 0.5$ (dashed line). Units: degrees day^{-1}

- the dust aerosols experiment in which the radiation parameterization included the radiative effects of dust aerosols, and
- the control experiment where the parameterization did not incorporate these effects.

a. Sea level pressure

Figure 7 shows the 48-, 96-, and 144-h sea level pressure forecasts ending at 1200 UTC 27 June, 29 June, and 1 July 1979, respectively, based on the control experiment and the dust aerosol experiment along with the observed fields.

On 27 June, the mean sea level pressure field in the aerosol experiment compares better with observation than the mean sea level pressure in the control experiment, particularly over the Saudi Arabian area. Over the Saudi Arabian region the mean sea level pressure field in the aerosol experiment is very similar to the observed field. The mean sea level pressure in the control experiment is about 4 mb higher than the observed field and that shown in the aerosol experiment over this region.

On 29 June, the Saudi heat low starts to form as a weak low-pressure trough over the eastern Rubalkhali Desert of Saudi Arabia. This was the first sign of the Saudi heat low since 26 June. The control experiment does not show the heat low, but maintains a thermal trough over the Rubalkhali Desert as a part of the monsoon heat low over northwest India. The aerosol experiment shows a fairly developed heat low over the southeastern Saudi Desert. The extension of the trough of low pressure over the eastern Mediterranean in this forecast is also in agreement with the observed pressure field. The control forecast does not show such northwestward extension of the trough.

On 1 July 1979, the heat low in the aerosol experiment forecast is in good agreement with the observations. The simulated strong Saudi heat low and the extension of the heat trough over the Gulf region and eastern Mediterranean is similar to the observed one. The monsoon low over northwest India was also well predicted in this experiment. The control experiment on the other hand did not simulate well either the Saudi heat low or the extension of the trough to the eastern Mediterranean region. As a result, the isobaric pattern shifted and the forecast pressure gradients weakened over the region. The monsoon low over northwest India was also much weaker in this forecast.

From the above it appears that the radiative effects of dust aerosol in the dust layer over the Rubalkhali Desert and the neighboring vicinity are a significant factor in the formation and intensification of the Saudi heat low. Despite its failure to simulate the formation of a heat low, the control experiment maintained a weak thermal trough over the Rubalkhali Desert throughout the 6-day period, mainly as a result of sensible heat fluxes of the Rubalkhali Desert. The heat low, its intensity, and location could properly be simulated only when the radiative effects of dust aerosol were included.

To see the variations in the dust aerosol radiative effects with the thickness of dust layer, we monitored the mean sea level pressure to the east of the Rubalkhali Desert at 21°N and 52°E during a 6-day simulation. The center of the Saudi heat low, which formed during the period, was located near this point. Figure 8 shows the variations in the observed and forecast sea level pressure by the control and the aerosol experiments along with the height of the top and thickness of the dust layer, which were used for initialization of dust aerosols in the model. During the first 3 days, the dust layer over this area was rather shallow with a thickness of about 250 mb and its top extending only to about 700 mb. The layer was loaded heavily with dust aerosols during this period. During the last 3 days, the dust intensity in the layer became moderate and the depth of the dust layer increased to 350 mb with its top lifting to 600 mb.

The observed mean sea level pressure was almost constant during the first 3 days but gradually fell during the next 3 days. The low-level winds were quite strong during the dust outbreak period. The strong winds along with a reduction of solar radiation reaching the ground due to heavy dust appear to inhibit the deepening of the heat low. However, the radiative heating of the shallow dust layer below 700 mb was sufficient to maintain the heat low as a low-intensity trough during this period. The heat low intensified over the Rubalkhali Desert due to radiative heating as the intensity of the dust layer decreased and its thickness increased. This occurred in the period following the dust outbreak when the winds

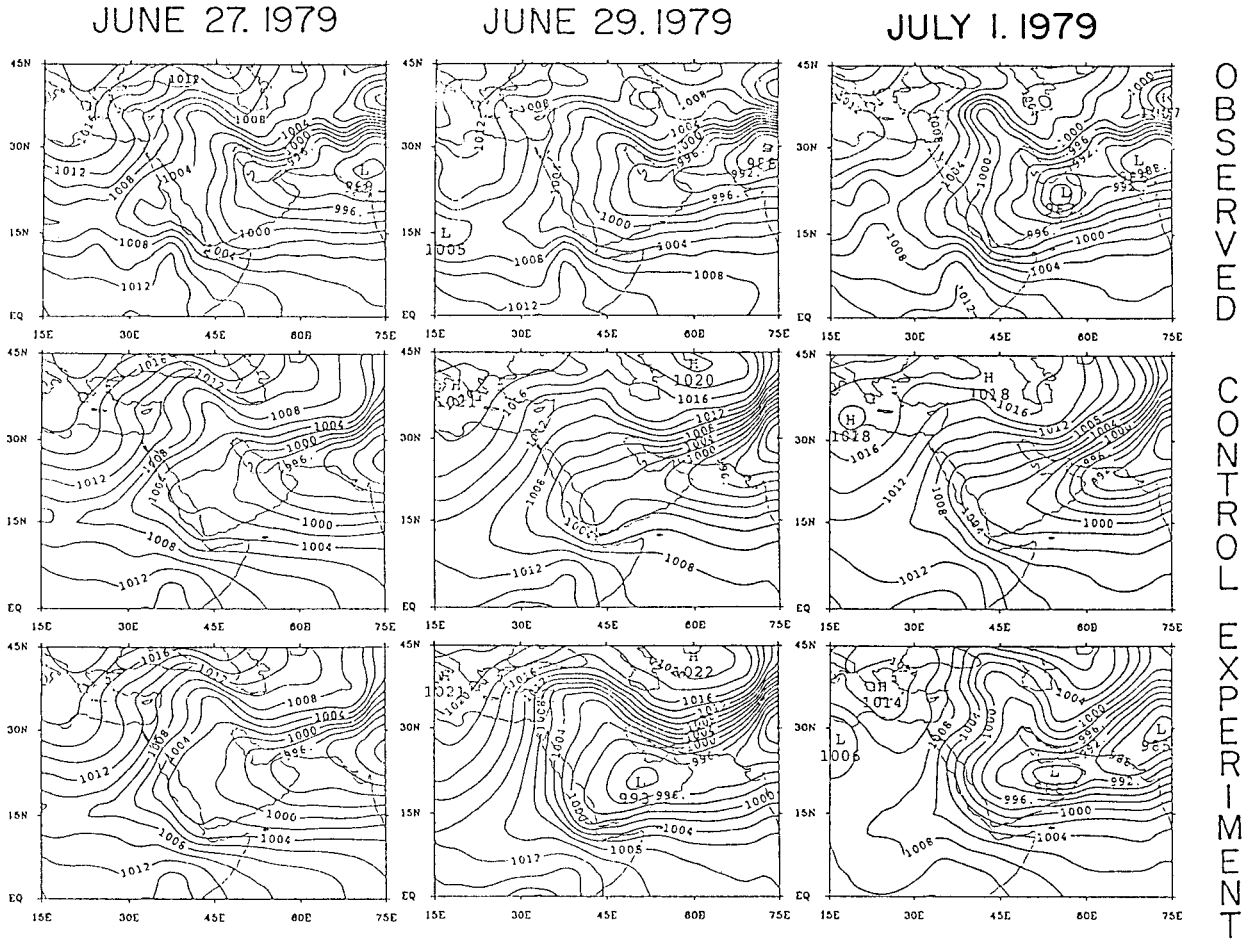

FIG. 7. Observed and forecast mean sea level pressure fields (mb) by the control and dust aerosol experiments at 1200 UTC on 27 June, 29 June, and 1 July 1979 at the end of 48-, 96-, and 144-h forecasts, respectively.

relaxed at low levels. More solar radiation could now reach the ground in the presence of light dust aerosol, resulting in more radiative heating of middle and lower levels and a pressure fall.

The dust aerosol experiment simulated these pressure changes over the Rubalkhali Desert area very well. During the first 4 days the mean sea level pressure in the aerosol experiment was nearly constant, and fell rather sharply during the last two days. The mean sea level pressure in this experiment during the last two days was about 2 mb lower than the observed pressure. The response of mean sea level pressure to the variations in the dust layer and its radiative effects over the region appears to be consistent with the observations.

The control experiment could not simulate the observed behavior of mean sea level pressure in this area. The pressure in the control experiment was nearly constant during the first 3 days and then rose gradually to 1003 mb on the last day, which was about 9 mb higher than its observed value.

b. Diurnal temperature change

Another parameter of importance over the desert region is the surface temperature. The desert of Saudi Arabia is characterized by a strong diurnal variation of surface temperature. The difference between the day and night temperatures can be 40°–50°C. The lowest layers of the atmosphere respond to the variations in temperature between day and night. The diurnal variations of temperature in the middle troposphere, though not strong, could be important for thermal stratification over the desert area and synoptic-scale systems at the surface. The thermal stratification of the air over the Saudi desert is seen to be the result of a thermal balance between the sensible heat flux from the surface, radiative heat of the dust aerosol, and the upper-air subsidence. To examine the role of dust aerosol radiative heating on the temperature at the surface and upper layers of the atmosphere, we looked into the mean diurnal mode of the temperature over a number of locations in the region. In Figs. 9a–c we show the 6-day mean observed and

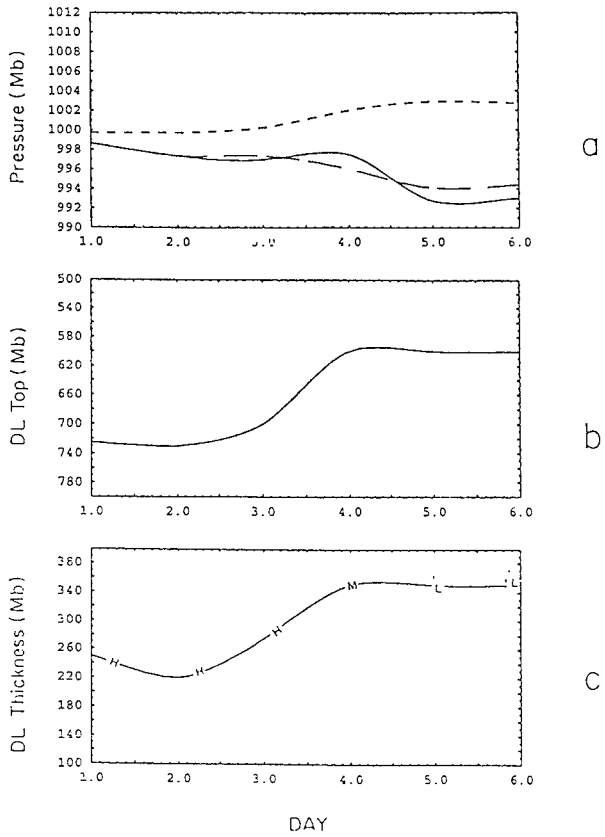

FIG. 8. The intensity of the heat low over Rubalkhali Desert (21°N, 52°E) in relation to the height of the top and thickness of the dust layer. In the top panel, the solid line shows observed mean sea level pressure of the heat low; the dashed line, the mean sea level pressure forecast by the aerosol experiment; and the dotted line, the mean sea level pressure forecast by the control experiment. The middle panel shows the pressure at the top of dust layer. The bottom panel shows the dust-layer thickness (in mb) along with its intensity (L = light, M = moderate, and H = heavy).

predicted diurnal mode of temperature of the control and aerosol experiments from 1000 to 400 mb over three locations: for example, (a) the Rubalkhali desert (21°N, 52°E), (b) the eastern Saudi Desert (26°N, 49°E), and (c) the northwest Arabian Sea (13°N, 54°E). The diurnal mode was obtained by subtracting the daily mean temperature values from its hourly mean values at different levels for the 6-day period.

Over the Rubalkhali Desert (Fig. 9a) the observed diurnal cycle of temperature has a positive value during the daytime between 0900 and 2000 UTC and negative during the night. The maximum occurs at around 1200 UTC, about 2–3 h after local noon, and the minimum during late night at around 0600 UTC. As a result of sensible heat flux from the hot desert surface during the day and longwave radiative cooling during the night, the diurnal cycle is strongest near the ground. The diurnal cycle in the upper levels has the same pattern but its amplitude becomes minimal above 800 mb. In the control experiment, the diurnal cycle at levels below 850 mb is similar to the observed. However, both the daytime maximum and nighttime minimum are about 1.5°C warmer than their observed values. Above about 750 mb, the diurnal cycle in the control experiment is out of phase with the observed cycle. The lowest negative diurnal change occurs at 700 mb at noontime. The diurnal cycle of temperature in the aerosol experiment has a phase and intensity very similar to those of the observed cycle. The radiative heating by dust aerosol improved the diurnal temperature cycle at the middle levels. Its amplitude also improved at the lower levels. The greatest improvement in the diurnal cycle was in its daytime component. The reduction of solar energy reaching the ground due to its absorption and scattering at upper levels by dust aerosol improved the diurnal temperature variations at lower as well as upper levels.

The behavior of observed and predicted diurnal temperature cycles at the central parts of the Saudi Desert (Fig. 9b) is similar to that of the Rubkhali Desert. The reduction of aerosol radiative warming in the control experiment appears to be most pronounced at 700 mb where the difference in the control and observed cycle is about 3°C. The diurnal cycle in the aerosol experiment is in good agreement with the observed cycle.

Over the northwest Arabian Sea (Fig. 9c), the observed diurnal cycle is strongest at about 800 mb. The temperature is higher than the daily mean by 0.5°C between 1200 and 1800 UTC from 850 to 700 mb, and lower by the same amount at 0000 UTC over this layer. The diurnal cycle at 1000 mb is rather weak as it is controlled by the prescribed sea surface temperature, which has a small diurnal range. The diurnal cycle in the control experiment is much different and relatively weaker. The daytime temperatures are higher by only 0.5°C at 0600 UTC at the surface level. There is no significant diurnal change over the middle levels. In contrast, the diurnal cycle in the aerosol experiment resembles the observed cycle. The diurnal cycle is strongest around 800 mb where temperatures are higher than their daily mean and occur between 1200 and 1800 UTC. The lower temperature of the same order, however, occurs at a lower level of 900 mb at 0000 UTC.

The difference between the diurnal cycle predicted by the control and aerosol experiments shows that during the daytime the dust aerosol radiative heating resulted in about 1.0°C warming between 850 and 600 mb and a small cooling (less than 0.5°C) below 850 mb. The presence of dust aerosol over the Arabian Sea thus seems to warm the layers above the monsoon flow and to slightly cool the lower levels, thus intensifying the low-level inversion over the area. The high temperatures at the middle levels are due to radiative heating resulting from absorption of solar radiation by the dust aerosol. The low temperatures at lower levels are due to the reduction of solar radiation by dust aerosol absorption and scattering in the upper layers.

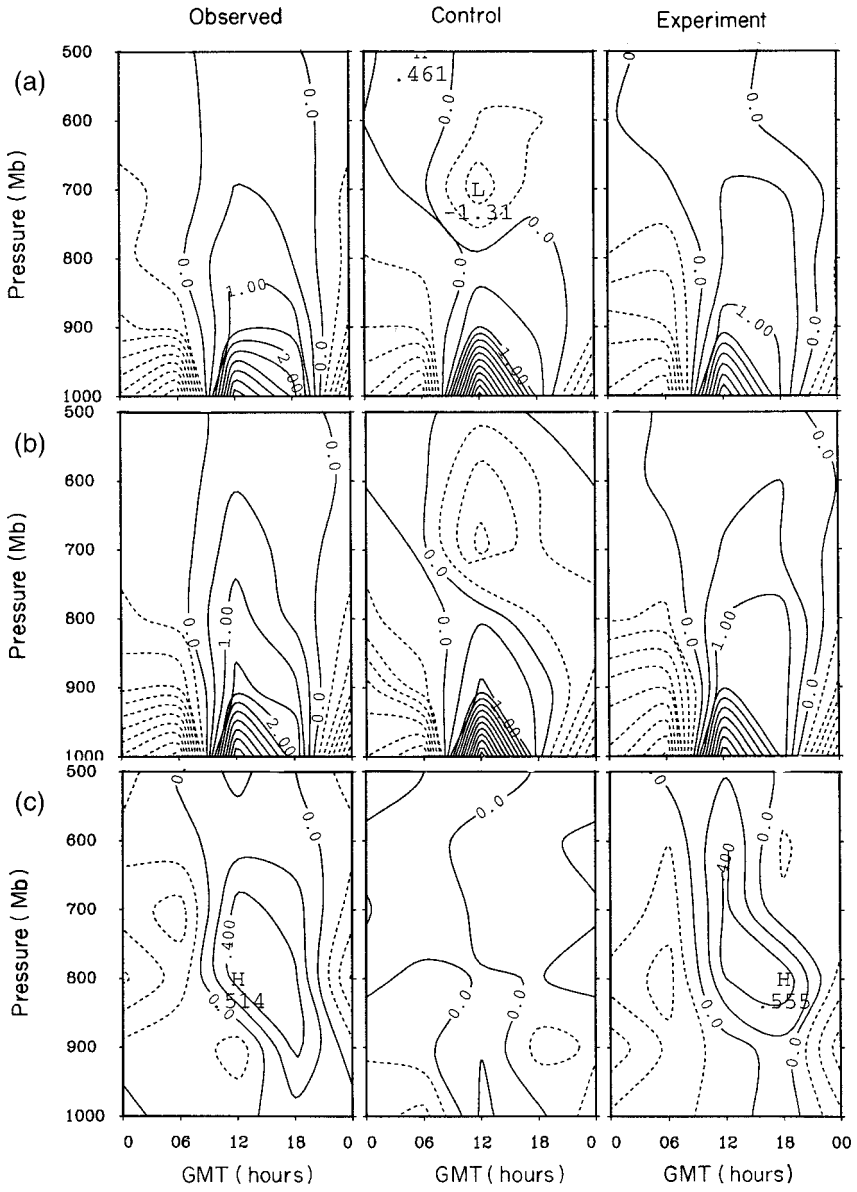

FIG. 9. Six-day composite diurnal mode of the observed and forecast temperature by the control and aerosol experiments at (a, upper panel) Rubalkhali Desert (21°N, 52°E), (b, middle panel) eastern Saudi Desert (26°N, 49°E), and (c, bottom panel) northwest Arabian Sea (13°N, 54°E). Contours show differences in °C between hourly mean temperature and daily mean temperature.

c. Diurnal variations of the Somali jet and land and sea breeze

In a detailed observational study using a network of double theodolite pilot balloon observations that were made 4–8 times a day, Ardanuy (1979) noted that the Somali jet over Africa experiences a pronounced diurnal change. He observed that the winds were strongest in the early morning hours and weakest in the late afternoon hours. With mean wind of 25 m s^{-1} in the early morning and 10 m s^{-1} in the late afternoon, the diurnal change is of the order of 15 m s^{-1} and the diurnal mean wind is also of the same order.

This picture, however, has been noted to reverse itself over the open ocean south of the Saudi Arabian peninsula. MONEX observations of 1979 (based on composites of dropwindsonde data) show that the late afternoon mean wind at around 9°N and 57°E is about 18 m s^{-1}, whereas the early morning composites show a mean wind of around 8 m s^{-1}. We observed that the winds simulated by the model described in this paper did exhibit an afternoon maximum at 850 mb at 10°N

and 58°E where the aerosol effects were incorporated in the radiation code. The winds at 850 mb at this location were slower when the aerosol effects were excluded in the radiative transfer algorithms. We have arrived at the following interpretation for this diurnal change. In the afternoon hours, the radiative flux convergence leads to a net temperature increase in the middle troposphere, whereas in the lower troposphere there is a net decrease in temperature (Fig. 9) near the Saudi Arabian coast where dust aerosols are encountered. The south–north gradient of temperature and the westerly thermal wind are enhanced between the cooler air to the north and the warmer air to the south. This appears to reasonably account for the differences in the diurnal wind changes for the aerosol experiment and the control experiment.

The effect of dust aerosols over the coastal area, however, appears to reduce the land–sea thermal gradient during daytime with little effect on it during the night. As a result, its presence in the model weakens the forecast sea breeze but has practically no effect on the land breeze.

5. Summary and conclusions

Dust aerosols have been a subject of discussion for many years, since Charney (1975) noted that the Arabian and Saharan Deserts exhibit radiative sink characteristics. Since then several field experiments over most of the deserts of the world have been conducted. One of these experiments (MONEX-79) documented the radiation budget over the Saudi Desert during the summer. The radiative heating of dust aerosols was found to contribute to the energy budget over the desert in a significant way, mainly at solar wavelengths. However, the effect of dust on the synoptic-scale systems and diurnal cycle over the region was not fully understood.

To study the effect of dust aerosols on the synoptic-scale system, a radiative transfer scheme for dust aerosols based on the two-stream Delta-Eddington approximation for shortwave radiation was included in the FSU model. The radiative transfer algorithim, based on a band model, thus includes treatments for clear-sky, cloudy-sky, and dust-laden atmospheric conditions. The satellite and horizontal visibility observations over the region of Saudi Arabia were used to identify and locate the dust layer. The dust aerosol properties (i.e., single-scattering albedo, asymmetry functions, and optical depths) used in the study were based on the long-term studies of dust aerosol characteristics by d'Almeida (1987) and Ackerman and Chung (1992). The period of 26 June–1 July 1979 was selected as the period of study, since 26–28 June was characterized by a heavy dust episode over the region, and 29 June–1 July was characterized by moderate to light dust. During these periods intensive observations were available from MONEX-79 on atmospheric variables like temperature, wind and moisture, surface temperature, and surface albedo.

The heat low shows a change in its intensity during and after the dust storm episode. A comparison of the results of the aerosol experiment with the control experiment shows that the impact of dust aerosols on the heat low can be summarized as follows: the dust aerosol radiative heating is an important factor in the development of a heat low over Saudi Arabia. The sensible heat flux from the hot desert surface results in the formation of a weak trough of low pressure as observed in the control experiment over the Rubalkhali Desert. Only when the dust aerosol radiative heating was included in the model did the heat low intensify properly with its strength comparable to the observed low. It appears that in spite of surface sensible heat fluxes, the mixing due to strong winds blowing from the north does not allow the intensification of the heat low. The inclusion of dust aerosol radiative effects, which result in warming over the lower troposphere throughout the dust-layer depth, offsets the cooling effect of strong winds and results in proper intensification of the heat low.

It seems that there is a 1-day lag in time for the heat low to respond to the radiative heating occurring in the dust layer. The heat-low trough over the Mediterranean region developed in the middle troposphere due to aerosol warming on 28 June. A pressure fall of 5 mb occurred 1 day later on 29 June 1979.

The diurnal mode of temperature over the desert shows the importance of dust aerosols in extending the diurnal cycle from the surface up to the middle-layer levels, with a warming occurring during the day and a cooling at night. The control experiment shows that the forecast diurnal cycle was not in phase with observations, whereas the aerosol experiment shows that the radiative heating of dust aerosol corrected the lower and middle troposphere diurnal cycle of temperature by 2°C. Moreover, the difference between the control and aerosol experiments shows that the amplitude of the diurnal temperature cycle is approximately doubled.

By comparing the diurnal variation of temperature between the observed, control, and aerosol experiments, it seems that the reduction of the sensible heat flux is due to a reduction of solar radiation reaching the surface as a result of the absorption and scattering by dust aerosols. This is balanced by the radiative heating of dust aerosols at low levels. This is true over the desert area where the dust layer extends to lower levels.

The role of dust aerosols over the Arabian Sea is to warm the middle levels between 800 and 600 mb and to cool the lower levels during daytime. This cooling occurs as a result of the reduction of solar radiance reaching low levels below the dust aerosol layer. The effect of the dust aerosol heating over the northwest Arabian Sea takes place in the 600–700-mb layer. The presence of the dust layer over the Arabian Sea thus results in the intensification of a low-level inversion in the monsoon flow.

The presence of dust aerosols over the region also

affects the strength of the Somali jet. The presence of the dust layer results in net warming of the middle troposphere and a cooling in the lower troposphere. The resultant strengthening of the south–north temperature gradient strengthens the westerly thermal wind and thus the Somali jet during the daytime. The dust layer also seems to weaken the sea breeze but does not have any significant effect on the land breeze.

Acknowledgments. The research reported here was funded by NSF Grant No. ATM9312537 and NOAA Grant No. NA56GP0013.

APPENDIX

Two-Stream Delta-Eddington Approximation and Numerical Solution of the Radiative Transfer Equation

The radiative transfer equation [Eq. (4), section 2) for diffusive radiation independent of an azimuthal angle is

$$\mu\frac{dI(\tau,\,\mu)}{d\tau} = -I(\tau,\,\mu) + \frac{\tilde{\omega}}{2}\int_{-1}^{1} I(\tau,\,\mu')P(\mu,\,\mu')\,d\mu' + \frac{\tilde{\omega}}{4\pi}S_0P(\mu,\,\mu_0)e^{-\tau/\mu_0}, \tag{A1}$$

where μ = cosine of zenith angle; τ = optical depth (of dust layer); $\tilde{\omega}$ = single-scattering albedo; $I(\tau\ \mu)$ = diffuse radiance from direction μ, through medium with optical depth τ; $P(\mu,\,\mu')$ = phase function describing the angular distribution of scattered radiation (i.e., proportion of radiation coming from direction μ' scattered to direction μ); and S_0 = direct solar radiation.

To solve Eq. (A1), the radiative intensity $I(\tau,\,\mu)$ and phase function $P(\mu,\,\mu')$ are represented in terms of Legendre polynomials as

$$I(\tau,\,\mu) = \sum_{l=0}^{\infty} I_l(\tau)P_l(\mu), \tag{A2}$$

$$P(\mu,\,\mu') = \sum_{l=0}^{\infty} \omega_l P_l(\mu)P_l(\mu'). \tag{A3}$$

Here $P_l(\mu)$ is a Legendre polynomial of degree l and I_l and ω_l are expansion coefficients.

In its normalized form the phase function satisfies the relation

$$\frac{1}{2}\int_{-1}^{1} P(\mu,\mu')\,d\mu' = 1. \tag{A4}$$

Under two-stream Delta-Eddington approximation, following Chandrasekhar (1960), the diffuse intensity and phase function are approximated by the first two Legendre polynomials, for example, $P_0(\mu) = 1$ and $P_1(\mu) = \mu$. With this from (A2), (A3), and (A4), we get

$$I(\tau,\,\mu) = I_0(\tau) + I_1(\tau)\mu$$
$$I(\tau,\,\mu') = I_0(\tau) + I_1(\tau)\mu' \tag{A5}$$

and

$$P(\mu,\,\mu') = 1 + 3g\mu\mu'$$
$$P(\mu,\,\mu_0) = 1 + 3g\mu\mu_0, \tag{A6}$$

where $I_0(\tau)$ and $I_1(\tau)$ are amplitudes of symmetric and asymmetric components of diffuse intensity, $I(\tau,\,\mu)$, and

$$g = \frac{1}{2}\int_{-1}^{1} P(\mu,\,\mu')\mu'\,d\mu'$$

is the asymmetry parameter.

Substituting for $I(\tau,\,\mu)$, $I(\tau,\,\mu')$ and $P(\mu,\,\mu')$ from (A5) and (A6) into (A1), we get two simultaneous equations:

$$\frac{dI_1}{d\tau} = -3(1-\tilde{\omega})I_0 + \frac{3\tilde{\omega}}{4\pi}S_0e^{-\tau/\mu_0}, \tag{A7}$$

$$\frac{dI_0}{d\tau} = -(1-\tilde{\omega}g)I_1 + \frac{3\tilde{\omega}}{4\pi}g\mu_0S_0e^{-\tau/\mu_0}. \tag{A8}$$

Assuming the single-scattering albedo $\overline{\omega}$ and the asymmetry factor g to be independent of optical depth τ, the solution for Eqs. (A7) and (A8) is given by

$$G = \pi I_0 = C_1e^{\lambda\tau} + C_2e^{-\lambda\tau} - \alpha e^{-\tau/\mu_0}, \tag{A9}$$

$$H = \frac{2}{3}\pi I_1 = -\kappa C_1e^{\lambda\tau} + \kappa C_2e^{-\lambda\tau} - \beta e^{-\tau/\mu_0}, \tag{A10}$$

where

$$\kappa = \frac{2}{3}\frac{\lambda}{1-\tilde{\omega}g},$$

$$\alpha = \frac{3}{4}S_0\tilde{\omega}\frac{(1+g(1-\tilde{\omega}))}{\left(\frac{1}{\mu_0^2}-\lambda^2\right)},$$

$$\beta = \frac{1}{2}\frac{S_0}{\mu_0}\tilde{\omega}\frac{(1+3g(1-\tilde{\omega})\mu_0^2)}{\left(\frac{1}{\mu_0}-\lambda^2\right)},$$

$$\lambda^2 = 3(1-\tilde{\omega})(1-\tilde{\omega}g),$$

and C_1 and C_2 are constants to be determined.

The upward and downward diffuse irradiances across a horizontal plane are given by

$$F\uparrow = \int_0^{2\pi}\int_0^{-1} \mu' I\,d\mu'\,d\theta = \int_0^{2\pi}\int_0^{-1} \mu'(I_0+\mu' I_1)\,d\mu'\,d\theta = \pi I_0 - \frac{2}{3}\pi I_1 = G - H, \tag{A11}$$

$$F\downarrow = \int_0^{2\pi}\int_0^1 \mu' I \, d\mu' \, d\theta$$
$$= \int_0^{2\pi}\int_0^1 \mu'(I_0 + \mu' I_1) \, d\mu' \, d\theta$$
$$= \pi I_0 + \frac{2}{3}\pi I_1 = G + H, \quad \text{(A12)}$$

where $G = \pi I_0$ and $H = (2/3)\pi I_1$ are symmetric and asymmetric components of flux of diffuse radiance, respectively.

If we know the value of the single-scattering albedo ($\tilde{\omega}$), the asymmetry factor (g), the solar constant (S_0), and the optical depth (τ), then we can calculate the flux of scattered radiation and thus heating or cooling due to it, provided we know the constants C_1 and C_2. The constants C_1 and C_2 are calculated numerically by dividing the dust layer into $N - 1$ sublayers as in Fig. A1.

In Fig. A1, the top of the dust layer is at level 1 and its bottom is at level N. The ith sublayer lies between levels i and $i + 1$ and has a single-scattering albedo $\overline{\omega}_i$ and an asymmetry factor g_i, and τ_i is the optical depth of the dust layer at level i. At level 1, the top of dust layer, $\tau_1 = 0$.

The solutions (A9) and (A10) for layer i may be written as

$$G_i = C_1^i e^{\lambda_i \tau} + C_2^i e^{-\lambda_i \tau} - \alpha_i e^{-\tau/\mu_0}, \quad \text{(A13)}$$
$$H_i = -\kappa_i C_1^i e^{\lambda_i \tau} + \kappa_i C_2^i e^{-\lambda_i \tau} - \beta_i e^{-\tau/\mu_0}. \quad \text{(A14)}$$

To evaluate the constants C_1^i and C_2^i over $N - 1$ layers, we need to formulate 2 $(N - 1)$ equations. Out of these, $2(N - 2)$ equations are determined from the consideration of continuity of upward and downward fluxes across interface levels 2 to $N - 1$. The remaining two equations are determined from the top and bottom boundary conditions as follows: (i) At the top boundary

$$G_1(0) + H_1(0) = F_0\downarrow, \quad \text{(A15)}$$

where $F_0\downarrow$ is the downward diffused radiative flux at level 1 (at $\tau = 0$).

(ii) At the bottom of the atmosphere the upward-directed radiance is the sum of the upward diffuse flux and the upward-reflected downward flux, for example,

$$F_N\uparrow = G_{N-1}(\tau_N) - H_{N-1}(\tau_N) - A[G_{N-1}(\tau_N) + H_{N-1}(\tau_N) + \mu_0 S_0 e^{-\tau_N/\mu_0}], \quad \text{(A16)}$$

where A is the ground surface albedo and τ_N is total optical depth of dust layer.

This results in the following set of $2N$ equations:

$$\begin{aligned}
&G_1(0) + H_1(0) = F_0\downarrow && \text{(upper boundary)}\\
&\left.\begin{aligned}
&G_1(\tau_2) + H_1(\tau_2) - G_2(\tau_2) - H_2(\tau_2) = 0\\
&G_1(\tau_2) - H_1(\tau_2) - G_2(\tau_2) + H_2(\tau_2) = 0\\
&\quad\vdots\\
&G_i(\tau_{i+1}) + H_i(\tau_{i+1}) - G_{i+1}(\tau_{i+1}) - H_{i+1}(\tau_{i+1}) = 0\\
&G_i(\tau_{i+1}) - H_i(\tau_{i+1}) - G_{i+1}(\tau_{i+1}) + H_{i+1}(\tau_{i+1}) = 0\\
&\quad\vdots\\
&G_{N-2}(\tau_{N-1}) + H_{N-2}(\tau_{N-1}) - G_{N-1}(\tau_{N-1}) - H_{N-1}(\tau_{N-1}) = 0\\
&G_{N-2}(\tau_{N-1}) - H_{N-2}(\tau_{N-1}) - G_{N-1}(\tau_{N-1}) + H_{N-1}(\tau_{N-1}) = 0
\end{aligned}\right\} && \text{(interface)}\\
&\quad\vdots\\
&(1 - A)G_{N-1}(\tau_N) - (1 + A)H_{N-1}(\tau_N) - A\mu_0 S_0 e^{-\tau_N/\mu_0} = F_N\uparrow && \text{(lower boundary).}
\end{aligned} \quad \text{(A17)}$$

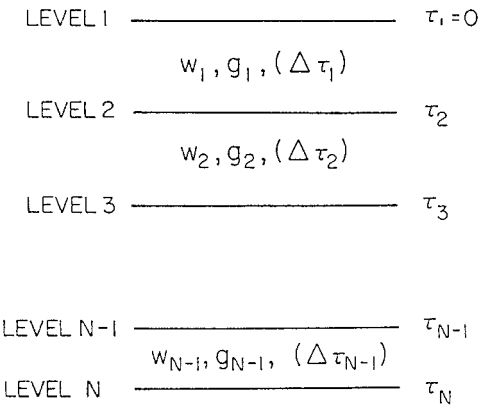

FIG. A1. Vertical distribution of layers and dust aerosol parameters, $\overline{\omega}$, g, and τ for the radiative transfer model.

This may be written as the following set of $2(N-1)$ simultaneous equations:

$$
\begin{aligned}
&(1-\kappa_1)C_1^1 + (1+\kappa_1)C_2^1 = \alpha_1 + \beta_1 + F_0{\downarrow}\\
&(1-\kappa_1)e^{\lambda_1\tau_2}C_1^1 + (1+\kappa_1)e^{-\lambda_1\tau_2}C_2^1 - (1-\kappa_2)e^{\lambda_2\tau_2}C_1^2 - (1+\kappa_2)e^{-\lambda_2\tau_2}C_2^2 = (\alpha_1+\beta_1-\alpha_2-\beta_2)e^{-\tau_2/\mu_0}\\
&(1+\kappa_1)e^{\lambda_1\tau_2}C_1^1 + (1-\kappa_1)e^{-\lambda_1\tau_2}C_2^1 - (1+\kappa_2)e^{\lambda_2\tau_2}C_1^2 - (1-\kappa_2)e^{-\lambda_2\tau_2}C_2^2 = (\alpha_1-\beta_1-\alpha_2+\beta_2)e^{-\tau_2/\mu_0}\\
&\qquad\vdots\\
&(1-\kappa_i)e^{\lambda_i\tau_{i+1}}C_1^i + (1+\kappa_i)e^{-\lambda_i\tau_{i+1}}C_2^i - (1-\kappa_{i+1})e^{\lambda_{i+1}\tau_{i+1}}C_1^{i+1} - (1+\kappa_{i+1})e^{-\lambda_{i+1}\tau_{i+1}}C_2^{i+1}\\
&\quad = (\alpha_i+\beta_i-\alpha_{i+1}-\beta_{i+1})e^{-\tau_{i+1}/\mu_0}\\
&(1+\kappa_i)e^{\lambda_i\tau_{i+1}}C_1^i + (1-\kappa_i)e^{-\lambda_i\tau_{i+1}}C_2^i - (1+\kappa_{i+1})e^{\lambda_{i+1}\tau_{i+1}}C_1^{i+1} - (1-\kappa_{i+1})e^{-\lambda_{i+1}\tau_{i+1}}C_2^{i+1}\\
&\quad = (\alpha_i-\beta_i-\alpha_{i+1}+\beta_{i+1})e^{-\tau_{i+1}/\mu_0}\\
&\qquad\vdots\\
&(1-\kappa_{N-2})e^{\lambda_{N-2}\tau_{N-1}}C_1^{N-2} + (1+\kappa_{N-2})e^{-\lambda_{N-2}\tau_{N-1}}C_2^{N-2} - (1-\kappa_{N-1})e^{\lambda_{N-1}\tau_{N-1}}C_1^{N-1} - (1+\kappa_{N-1})e^{-\lambda_{N-1}\tau_{N-1}}C_2^{N-1}\\
&\quad = (\alpha_{N-2}+\beta_{N-2}-\alpha_{N-1}-\beta_{N-1})e^{-\tau_{N-1}/\mu_0}\\
&(1+\kappa_{N-2})e^{\lambda_{N-2}\tau_{N-1}}C_1^{N-2} + (1-\kappa_{N-2})e^{-\lambda_{N-2}\tau_{N-1}}C_2^{N-2} - (1+\kappa_{N-1})e^{\lambda_{N-1}\tau_{N-1}}C_1^{N-1} - (1-\kappa_{N-1})e^{-\lambda_{N-1}\tau_{N-1}}C_2^{N-1}\\
&\quad = (\alpha_{N-2}-\beta_{N-2}-\alpha_{N-1}+\beta_{N-1})e^{-\tau_{N-1}/\mu_0}\\
&[(1-A)+(1+A)\kappa_{N-1}]e^{\lambda_N\tau_N}C_1^{N-1} + [(1-A)-(1+A)\kappa_{N-1}]e^{-\lambda_N\tau_N}C_2^{N-1}\\
&\quad = [(1-A)\alpha_{N-1} - (1+A)\beta_{N-1} + A\mu_0 S_0]e^{-\tau_N/\mu_0} + F_N{\uparrow}. \qquad \text{(A18)}
\end{aligned}
$$

The set of equations (A18) is solved by writing it in the form:

$$\mathbf{AC} = \mathbf{F}, \qquad \text{(A19)}$$

where $\mathbf{A}$ is a pentadiagonal matrix of coefficients of C_1^i and C_2^i. Here $\mathbf{C}$ and $\mathbf{F}$ are column vectors of the constants C_1^i and C_2^i and forcing functions on the right-hand sides of (A18), respectively.

With C_1^i and C_2^i known, the upward and downward fluxes of scattered radiance are obtained as

$$F_i{\uparrow} = G_i - H_i, \qquad \text{(A20)}$$

$$F_i{\downarrow} = G_i + H_i. \qquad \text{(A21)}$$

The total downward radiative flux across any level is given by

$$F = F_i{\downarrow} - F_i{\uparrow} + \mu_0 S_0 \mathrm{e}^{-\tau_i/\mu_0} \qquad \text{(A22)}$$

The heating rates are given by

$$\frac{dT}{dt} = \frac{g}{c_p}\frac{dF}{dp}. \qquad \text{(A23)}$$

REFERENCES

Ackerman, S. A., and S. K. Cox, 1982: The Saudi Arabian heat low: Aerosol distribution and thermodynamic structure. *J. Geophys. Res.,* **87,** 8991–9002.

——, and H. Chung, 1992: Radiative effects of airborn dust on regional energy budgets at the top of the atmosphere. *J. Appl. Meteor.,* **31,** 223–233.

Ardanuy, P., 1979: On the observed diurnal oscillations of the Somali jet. *Mon. Wea. Rev.,* **107,** 1694–1700.

Blake, D. W., T. N. Krishnamurti, S. V. Low-Nam, and J. S. Fein, 1983: Heat low over Saudi Arabian desert during May 1979 (Summer MONEX). *Mon. Wea. Rev.,* **111,** 1759–1775.

Businger, J. A., J. C. Wyngaard, Y. Izumi, and E. F. Bradley, 1971: Flux-profile relationships in the atmospheric surface layer. *J. Atmos. Sci.,* **28,** 181–189.

Carlson, T. N., and S. G. Benjamin, 1980: Radiative heating rates for Saharan dust. *J. Atmos. Sci.,* **37,** 193–213.

Chandrasekhar, S., 1960: *Radiative Transfer*. Dover Publishing, 393 pp.

Charney, J. G., 1975: Dynamics of deserts and droughts in the Sahara. *Quart. J. Roy. Meteor. Soc.,* **101,** 193–202.

Coakley, J. A., Jr. and P. Chýlek, 1975: The two-stream approximation in radiative transfer: Including the angle of the incident radiation. *J. Atmos. Sci.,* **32,** 409–418.

d'Almeida, G. A., 1987: On the variability of desert aerosol radiative characteristics. *J. Geophys. Res.,* **92,** 3017–3026.

Harshvardhan, and T. G. Corsetti, 1984: Longwave parameterization for the UCLA/GLAS GCM. NASA Tech. Memo. 86072, 52 pp. [Available from Goddard Space Flight Center, Greenbelt, MD 20771.]

Joseph, J. H., W. J. Wiscombe, and J. A. Weinman, 1976: The delta-Eddington approximation for radiative flux transfer. *J. Atmos. Sci.,* **33,** 2452–2459.

Karyampudi, V. M., and T. N. Carlson, 1988: Analysis and numerical

simulation of the Saharan air layer and its effect on easterly wave disturbances. *J. Atmos. Sci.,* **45,** 3102–3136.

Krishnamurti, T. N., S. Low-Nam, and R. Pasch, 1983: Cumulus parameterization and rainfall rates II. *Mon. Wea. Rev.,* **111,** 815–828.

——, A. Kumar, K. S. Yap, A. P. Datoor, N. Davidson, and J. Sheng, 1990: Performance of a high-resolution mesoscale tropical prediction model. *Advances in Geophysics,* Vol. 32, Academic Press, 133–286.

Lacis, A. A., and J. E. Hansen, 1974: A parameterizaiton for the absorption of solar radiation in the earth's atmosphere. *J. Atmos. Sci.,* **31,** 118–133.

Meador, W. E., and W. R. Weaver, 1980: Two-stream approximation to radiative transfer in planetary atmospheres: A unified description of existing methods and a new improvement. *J. Atmos. Sci.,* **37,** 630–643.

Smith, E. A., 1986: The structure of the Arabian heat low. Part II: Bulk tropospheric heat budget and implications. *Mon. Wea. Rev.,* **114,** 1084–1102.

——, S. A. Ackerman, S. K. Cox, and T. H. Vonder Haar, 1980: Summer MONEX high altitude aircraft radiation measurement. Dept. of Atmospheric Science, Colorado State University, Fort Collins, CO, 84 pp.

Sokolik, I. N., and G. S. Golitsyn, 1993: Investigation of optical and radiative properties of dust aerosol. *Atmos. Environ.,* **27A,** 2509–2517.

Tegen, I., A. A. Lacis, and I. Fung, 1996: The influence on climate forcing of mineral aerosols from disturbed soils. *Nature,* **380,** 419–422.

Wiscombe, W. J., 1977: The delta-Eddington approximation for a vertical inhomogenous atmosphere. NCAR Tech. Note TN-121-STR, NCAR, Boulder, CO, 66 pp. [NTIS PB 270618.]

Wiscombe, W. N., 1976: Extension of the doubling method to inhomogenous sources. *J. Quant. Spectrosc. Radiat. Transfer,* **16,** 477–489.